doi:10.1093/plphys/kiab295 PLANT PHYSIOLOGY 2021: 187: 873–885

Plant Physiology®

Research Article

Seawater exposure causes hydraulic damage in dying Sitka-spruce trees

Hongxia Zhang ,[1,2,3] Xinrong Li,[1] Wenzhi Wang ,[3,4] Alexandria L. Pivovaroff ,[3] Weibin Li ,[3,5] Peipei Zhang,[3] Nicholas D. Ward ,[6,7] Allison Myers-Pigg ,[5] Henry D. Adams,[8] Riley Leff,[3] Anzhi Wang,[2] Fenghui Yuan,[2] Jiabing Wu,[2] Steve Yabusaki ,[9] Scott Waichler ,[9] Vanessa L. Bailey ,[10] Dexin Guan ,[2,*,†] and Nate G. McDowell[3,11,†]

1 Shapotou Desert Research and Experiment Station, Northwest Institute of Eco-Environment and Resources, Chinese Academy of Sciences, Lanzhou 730000, China
2 Key Laboratory of Forest Ecology and Management, Institute of Applied Ecology, Chinese Academy of Sciences, Shenyang 110016, China
3 Atmospheric Sciences and Global Change Division, Pacific Northwest National Laboratory, Richland, Washington 99354, USA
4 The Key Laboratory of Mountain Environment Evolution and Regulation, Institute of Mountain Hazards and Environment, Chinese Academy of Sciences, Chengdu 610041, China
5 State Key Laboratory of Grassland and Agro-ecosystems, Key Laboratory of Grassland Livestock Industry Innovation, Ministry of Agriculture and Rural Affairs, College of Pastoral Agriculture Science and Technology, Lanzhou University, Lanzhou 730020, China
6 Marine Sciences Laboratory, Pacific Northwest National Laboratory, Sequim, Washington 98382, USA
7 School of Oceanography, University of Washington, Seattle, Washington 98195, USA
8 School of the Environment, Washington State University, Pullman, Washington 99164-2812, USA
9 Earth Systems Science, Pacific Northwest National Laboratory, Richland, Washington 99354, USA
10 Biological Sciences Division, Pacific Northwest National Laboratory, Richland, Washington 99354, USA
11 School of Biological Sciences, Washington State University, Pullman, Washington 99164-4236, USA

*Author for communication: dxguan@iae.ac.cn
†Joint senior authors.

N.G.M., H.Z., D.G., W.W., and V.L.B. planned and designed the present study. H.Z., N.G.M., W.W., A.L.P., P.Z., W.L., N.W. conducted the field work and contributed to data collection, assisted by R.L., A.M.P. S.Y., S.W. and N.W. provided salinity data and modeled soil salinity. H.Z., N.G.M., and D.G. conducted the data analysis and interpretation. H.Z. and N.G.M. drafted the manuscript with contributions from all other authors. N.G.M. and D.G. agree to serve as the authors responsible for contact and ensure communication.
The author responsible for distribution of materials integral to the findings presented in this article in accordance with the policy described in the Instructions for Authors (https://academic.oup.com/plphys/pages/general-instructions) is: Dexin Guan (dxguan@iae.ac.cn).

Abstract

Sea-level rise is one of the most critical challenges facing coastal ecosystems under climate change. Observations of elevated tree mortality in global coastal forests are increasing, but important knowledge gaps persist concerning the mechanism of salinity stress-induced nonhalophytic tree mortality. We monitored progressive mortality and associated gas exchange and hydraulic shifts in Sitka-spruce (*Picea sitchensis*) trees located within a salinity gradient under an ecosystem-scale change of seawater exposure in Washington State, USA. Percentage of live foliated crown (PLFC) decreased and tree mortality increased with increasing soil salinity during the study period. A strong reduction in gas exchange and xylem hydraulic conductivity (K_s) occurred during tree death, with an increase in the percentage loss of conductivity (PLC) and turgor loss point (π_{tlp}). Hydraulic and osmotic shifts reflected that hydraulic function declined from seawater exposure, and dying trees were unable to support osmotic adjustment. Constrained gas exchange was strongly related to hydraulic damage at both stem and leaf levels. Significant correlations between foliar sodium (Na^+) concentration and gas exchange and key hydraulic parameters (K_s, PLC, and π_{tlp}) suggest that cellular injury related to the toxic effects of ion accumulation

Received May 11, 2021. Accepted June 9, 2021. Advance access publication June 22, 2021
© American Society of Plant Biologists 2021. All rights reserved. For permissions, please email: journals.permissions@oup.com

Downloaded from https://academic.oup.com/plphys/article/187/2/873/6307737 by guest on 18 April 2024

impacted the physiology of these dying trees. This study provides evidence of toxic effects on the cellular function that manifests in all aspects of plant functioning, leading to unfavourable osmotic and hydraulic conditions.

Introduction

Sea-level rise and storm surges caused by thermal expansion of seawater and glacial melting due to global warming have been recently documented (Meehl et al., 2005; Vermeer and Rahmstorf, 2009; Foster and Rohling, 2013; Jevrejeva et al., 2016). Sea-level rise can raise the soil salinity level of coastal areas due to increased tidal flooding, which strongly affects coastal ecosystem structure and function (Twilley et al., 2001; Thorne et al., 2018). These effects include the accelerating decline of coastal forests (Williams et al., 1999; Desantis et al., 2007; Doyle et al., 2010; Kirwan and Gedan, 2019) and coastal salt-marshes (Silliman et al., 2005). Salinity stress from seawater exposure affects plant carbon gain and water relations, subsequently impacting plant growth, reproduction, and survival (Hao et al., 2009; Abou Jaoude et al., 2013; Leopold et al., 2016; Liu et al., 2017). However, the hydraulic and carbon-related physiological mechanisms that underlie potential mortality mechanisms, particularly for nonhalophytic coastal tree species, remain elusive.

Impacts of salinity stress on plant carbon assimilation and water transport capacity have primarily been conducted in crops (Epstein et al., 1980; Munns and Gilliham, 2015) or salt-tolerant plants (i.e. halophytes such as mangroves, see Naidoo, 1987; Scholander, 2006), with little research on coastal nonhalophytes. Some coastal marsh and mangrove species have adapted to a wide range of saline environments, but this adaptability is not expected for the slightly more upland species that typically grow in freshwater environments. Sea-level-driven acceleration in coastal forest retreat and dramatic increases in tree mortality have been observed in coastal areas (Desantis et al., 2007; Langston et al., 2017; Kirwan and Gedan, 2019; Schieder and Kirwan, 2019). Therefore, it is imperative to understand the mechanism of salinity-induced tree mortality in such environments.

The hydraulic framework that predicts hydraulic failure and carbon starvation during mortality (McDowell et al., 2011; Adams et al., 2017) can be used to provide logical hypotheses regarding salinity-induced mortality. Hydraulic failure through loss of xylem function from embolism is a central pathway to mortality (Brodribb and Cochard 2009; Yao et al., 2021), which is typically assessed via percentage loss of xylem conductivity (PLC). Hydraulic failure can lead to tree death if it is extensive throughout the vascular system or may promote carbon starvation if it is localized enough and impacts carbon uptake (Gong et al., 2021). Carbon starvation is the process by which metabolic needs are not met due to reduced carbon supply rate, which like a hydraulic failure is nonlethal until a threshold is reached. Zhang et al. (2021b) recently observed extreme declines in nonstructural carbohydrate (NSC) content as Sitka-spruce trees (*Picea sitchensis*) approached death, suggesting that carbon starvation occurred during seawater exposure. However, how hydraulics shift during Sitka-spruce tree mortality is still unknown, but they may help explain the mechanisms of carbon starvation if it occurs.

The process of hydraulic failure during salinity stress is complicated. Soil salinity stresses plants in two phases: the osmotic phase where high concentrations of salts in the soil make it harder for roots to extract water, and the ionic phase where high concentrations of salts within the plant can be toxic (Munns and Tester, 2008). The osmotic phase is a rapid response of plants to salinity stress, while the ionic phase is slower because it takes time to accumulate ions. Osmotic imbalance under salinity stress reduces plant growth and survival (Munns and Tester, 2008; Horie et al., 2009; Mendez-Alonzo et al., 2016). The water potential in roots is lower than in the surrounding soils when plants grow in optimum environments. However, in saline environments, the water potential gradient between soil and roots is reduced or even inverted (Boursiac et al., 2005), thus whole-plant hydraulic conductance declines (Brodribb and Holbrook, 2003; Ewers et al., 2004). For example, standard seawater (described in Harvey, 1996) has an osmotic potential of −2.4 MPa. This reduction in belowground conductance can promote hydraulic failure if the water supply fails to meet the demand for extended periods (Sperry et al., 1988b; Melcher et al., 2001; Sobrado, 2001). Stomatal closure typically occurs to maintain osmotic pressure and xylem water potential under such conditions (Brodribb and Holbrook, 2003; Pedrero et al., 2014; Yang et al., 2021), leading to a strong reduction in photosynthesis (Burchett et al., 1984; Suárez and Medina, 2006). Thus, elevated soil salinity can promote hydraulic failure due to belowground constraints.

In addition to hydraulic failure, ion toxicity-induced limitations on gas exchange may promote mortality. Under conditions of salinity-induced osmotic imbalance, plants accumulate compatible solutes and ions to increase turgor potential (Munns, 1993, 2002). Plants preferentially utilize inorganic ions (i.e. Na^+) for osmotic adjustment rather than organic solutes from photosynthesis because of the minimized energetic cost (Arsova et al., 2020; Munns et al., 2020a). However, ions can accumulate to toxic concentrations as nonhalophytic plants in chronically saline soil are unable to exclude the extra salt (Munns et al., 2020b). Elevated ion concentrations can lead to cellular Na^+ toxicity, resulting in various impairments in cellular processes (Munns and Tester, 2008; Hauser and Horie, 2010). Initial effects of low salinity are recoverable, but long-term effects resulting from the accumulation of salt within expanded

Downloaded from https://academic.oup.com/plphys/article/187/2/873/6307737 by guest on 18 April 2024

leaves may not be recoverable (Yeo et al., 1991). For example, high Na^+ concentration could cause ionic (Na^+, potassium (K^+), and chloride ion (Cl^-)) imbalance in leaves and oxidative damage to photosystems and membranes (Parida and Das, 2005; Miller et al., 2010; Bose et al., 2017). These toxic effects potentially cause reductions in photosynthesis (Welfare et al., 2002).

Constrained tree growth and gas exchange of seawater-exposed forests have been reported by Wang et al. (2019) using wood carbon (C) isotopes ($\delta^{13}C$), which suggested that salinity-induced stomatal closure may constrain C assimilation. Thus, we speculate that the coordination of hydraulics and gas exchange is likely to have played a critical role in tree survival, with hydraulic conductance constraining plant gas exchange (Sack and Holbrook, 2006). To understand the mechanism of tree mortality in coastal areas exposed to seawater, we observed the dynamic death process of Sitka-spruce trees along a tidal creek in a coastal watershed in the Pacific Northwest USA where seawater culverts were breached in 2014, allowing tidal fluctuations to intrude into a previously freshwater dominated floodplain forest (Sengupta et al., 2019; Wang et al., 2019; Yabusaki et al., 2020). This ecosystem-scale manipulation allowed us to examine changes in gas exchange, hydraulic traits, and leaf ion concentration in Sitka-spruce trees with different crown conditions, over six months in 2019. Our specific goal was to uncover the hydraulic shifts throughout progressive mortality. We hypothesize that (1) hydraulic and osmotic functions change in response to seawater exposure; (2) constrained gas exchange under seawater exposure is related to stem hydraulic loss and leaf osmotic damage; and (3) hydraulic and osmotic decline is related to the toxic effects of ion accumulation under salinity stress.

Results

Soil porewater salinity and percentage of live foliated crown

Floodplain soil porewater salinity modeling results showed that soil salinity tends to fluctuate and increase from 2015 to 2019 (Figure 1a). Annual soil salinity was 4.32 PSU (practical salinity units) in 2015 and reached 7.41 PSU in 2019 as exposure to seawater accumulated over time. Mean measured porewater salinity was significantly increased along the river bank and the middle floodplain ($P < 0.05$, analysis of variance (ANOVA); Figure 1b) during the study period (from March to August 2019), but not near the hillslope ($P > 0.05$). Our target trees were selected along the river bank and the middle floodplain, where the salinity increased from 7.16 ± 1.46 and 7.96 ± 0.04 PSU in March to 13.90 ± 1.45 and 13.37 ± 1.7 PSU in August (Figure 1b). We found that percentage of live foliated crown (PLFC) declined rapidly while the number of dead trees increased from March to August 2019 ($P < 0.001$, ANOVA; Figure 1c), and PLFC (measured in March) was significantly inversely correlated with modeled porewater salinity (averaged from 2015 to 2019; $P = 0.02$; Figure 1d).

Hydraulics and gas exchange

Mean leaf water potential at predawn (Ψ_{pd}) and midday (Ψ_{md}) from March to August were −0.67 MPa and −1.15 MPa, respectively (Figure 2). PLFC showed no significant correlation with both Ψ_{pd} and Ψ_{md} (Figure 2), but it decreased significantly with decreasing A and native K_s ($P < 0.001$; Figure 3, A and B). The effects of seawater exposure on A and K_s were not significant among months (insert Figure 3, A and B). PLFC was lower for trees with higher native PLC ($P < 0.001$; Figure 4), with P_{50} averageing −3.69 MPa across wet (March) and dry (July) seasons ($P > 0.05$; insert Figure 4). PLC increased rapidly when PLFC was below 45% (Figure 4). PLFC was significantly correlated with pressure–volume (P–V) parameters including π_{tlp} and RWC_{tlp}, but not for π_0, ε, and saturated water content (SWC) (Figure 3; Supplemental Figure S1). Trees with lower PLFC had higher (less negative) π_{tlp}, with no significant differences in π_{tlp} across months (Figure 3C).

Relations across traits

Significant linear correlations were found among A, K_s, PLC, and π_{tlp} under seawater exposure (Figure 5). Specifically, A decreased significantly with decreasing g_s ($P < 0.001$; Figure 5A), and g_s decreased significantly with decreasing K_s ($P < 0.05$; Figure 5B), and K_s decreased with the increasing of PLC ($P < 0.01$; Figure 5C), and A decreased significantly with increasing (less negative) π_{tlp} ($P < 0.05$; Figure 5D). In addition, A, K_s, PLC, and π_{tlp} were significantly correlated with foliar Na^+ concentration (Figure 6), and A and K_s significantly decreased with increasing foliar Na^+ concentration ($P < 0.001$, $P < 0.05$, respectively; Figure 6, A and B), and PLC and π_{tlp} significantly increased with increasing foliar Na^+ concentration ($P < 0.05$; Figure 6, C and D).

We summarized crown mortality conditions (PLFC) with gas exchange (A) and hydraulic safety (PLC and π_{tlp}) traits into principal components analysis (PCA; Figure 7A). Using PCA, we found that the first PC (PC1) explained 88.2% of the total variance in four functional traits and the second PC (PC2) explained 6.4% of the total variance. Furthermore, we found that the first component of the PC axes (Dim 1) was significantly correlated with foliar Na^+ concentration ($P = 0.009$; Figure 7B).

Discussion

Constrained gas exchange under seawater exposure related to stem hydraulic loss and leaf osmotic damage

The Sitka-spruce trees located within a seawater-induced salinity gradient experienced declining crown conditions and ultimately died. Our data showed that the PLFC declined with decreasing photosynthetic rate (A) of spruce trees (Figure 3A), supporting the previous observations that gas exchange and growth were constrained under seawater exposure at this site (Wang et al., 2019). This is also consistent with previous observations of strong reductions in carbon assimilation rate and growth rates when plants are

Downloaded from https://academic.oup.com/plphys/article/187/2/873/6307737 by guest on 18 April 2024

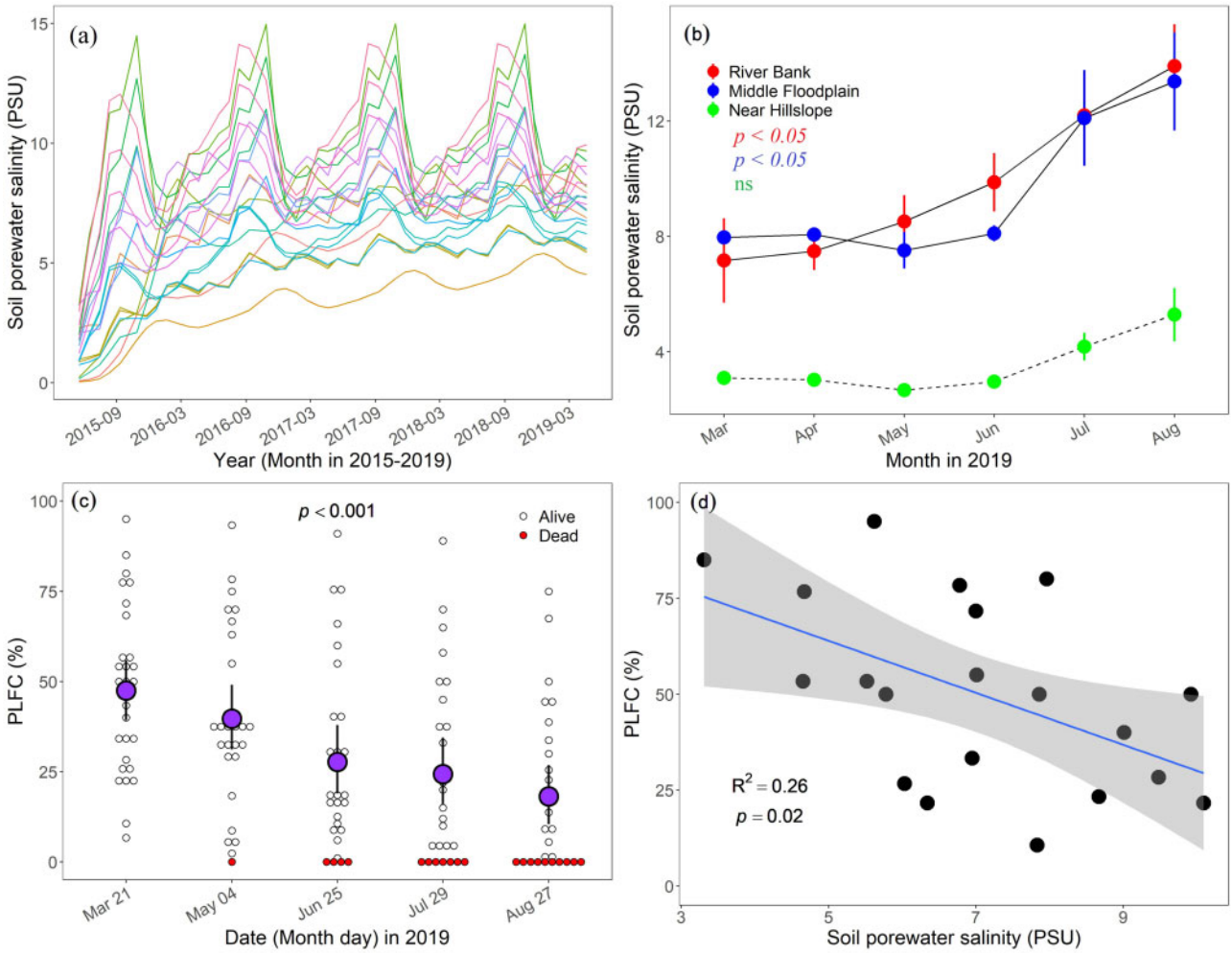

Figure 1 The dynamics of porewater salinity and PLFC over time. A, Modeled soil porewater salinity (PSU, practical salinity units) from May 2015 to April 2019. The color of lines represents the location of our target individual trees. B, Mean porewater salinity of the floodplain sites (River Bank, Middle Floodplain, and Near Hillslope) by month (March–August) in the year 2019 [mean porewater salinity significantly increased for River Bank and Middle Floodplain over the study period ($P < 0.05$; ANOVA)]. Error bars represent ±1 standard error ($n = 3$). C, The pPLFC declined and the number of dead trees increased rapidly over the study period (from March to August 2019; $P < 0.001$; ANOVA). Black hollow circles and black circles filled with red represent alive and dead trees, respectively. The circles filled with purple represent the mean PLFC of all individuals. Error bars represent ±1 standard error ($n = 28$) of observed values. D, Relationship between PLFC and soil porewater salinity. The confidence intervals of linear or nonlinear regression were shown in light gray color. The points represent the individual trees. The coefficient of determination and *P*-value are also shown.

exposed to high salinity substrates (Ball and Farquhar, 1984; Laura et al., 2007). The constrained photosynthetic CO_2 assimilation under salinity stress was caused by the reduction in stomatal conductance and consequent restriction of CO_2 diffusion (Brugnoli and Lauteri, 1991; Delfine et al., 1999; James et al., 2002), as reflected in our *gs* observations (Figure 5A). The decline in *gs* is considered to be an important mechanism for salinity tolerance that reduces water loss in plants (Moradi and Ismail, 2007; Zhang et al., 2021a). We also found that *gs* was positively correlated with stem hydraulic conductivity (K_s), and the K_s decreased with the increase in PLC under seawater exposure (Figure 5, B and C). This suggests that the constrained gas exchange under seawater exposure was partly attributed to the hydraulic function loss at the stem level. Loss of stem K_s could result from greater vulnerability to xylem embolism under high osmotic pressure after seawater exposure. This is consistent with previous experimental results that NaCl addition decreased hydraulic conductivity in mangroves (Kaneko et al., 2015). Furthermore, it is interesting that *A* decreased with increasing (more positive) π_{tlp}, and the increasing (less negative) π_{tlp} was tightly associated with an increase in foliar Na^+ concentration (Figure 5, D and D), suggesting an increase in salinity stress that impacted photosynthetic capacity by impeding osmotic function at leaf level. Na^+ toxicity in leaves induced leaf osmotic damage could be another reason for the decline in gas exchange, which is consistent with the results of Li et al. (2021), who reported ion toxicity as part of the process in decreased photosynthetic capacity in spruce trees.

Downloaded from https://academic.oup.com/plphys/article/187/2/873/6307737 by guest on 18 April 2024

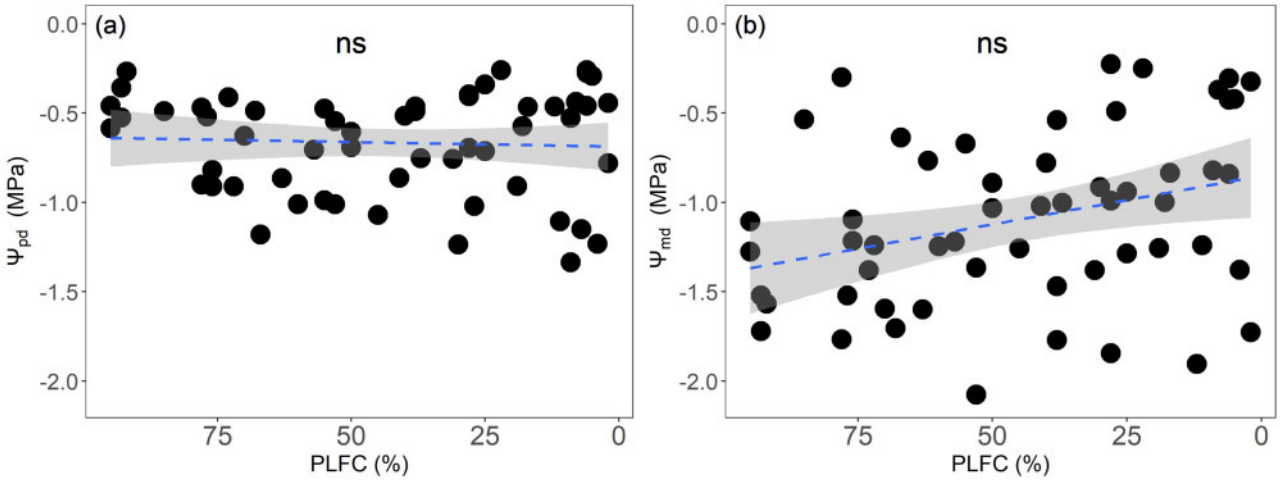

Figure 2 Relationships of crown mortality and water potential. Relationship between predawn water potential (Ψ_{pd}; A) and midday water potential (Ψ_{md}; B), and PLFC. Each point is the average of three branches. A linear model is fitted to the data in each panel. The confidence intervals of linear regressions are shown in light gray color. The results were not significant (ns; $P > 0.05$).

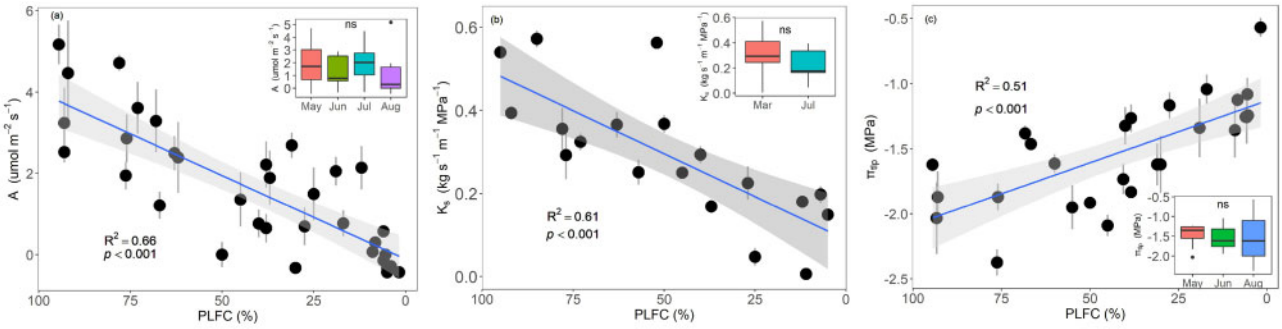

Figure 3 Relationships of crown mortality and three tree key functional traits. Relationship between carbon assimilation rate (*A*; A), sapwood-specific hydraulic conductivity (K_s; B), and turgor loss point (π_{tlp}; C) and PLFC. Each point is the average $A/K_s/\pi_{tlp}$ of two to three stems per individual tree. Vertical bars represent ±1 standard error. Inset: The figure shows boxplots representing interquartile range and median values for $A/K_s/\pi_{tlp}$ across months. Whiskers extend to 1.5 times box size above and below the median; any observations outside this range are denoted as individual points. Differences across months were not significant for *A*, K_s, and π_{tlp} (ns; $P > 0.05$; ANOVA). A linear model is fitted to the data in each panel. The confidence intervals of the regressions are shown in light grey color. The coefficients of determination and *P*-values are also shown in each panel.

The carbon assimilation rate became negative when trees were near death (Figure 3A), suggesting that carbon gain via photosynthesis was less than carbon loss via autotrophic respiration during their last surviving weeks. The declines in carbon gain were consistent with the results by Zhang et al. (2021b) who reported large declines in nonstructural carbohydrates and starch was almost completely consumed as the trees approached death at the same study site. In this study, the seawater-induced damage was apparent when PLFC <45%, rather than in leaf water potential (Figures 2 and 4), and the crown started to decline even when the trees had low PLC (PLC remained <20% until PLFC declined to 45%; Figure 4). The extreme depletion in nonstructural carbohydrates coupled with the relatively minor PLC experienced by the trees suggests that carbon starvation might be more pronounced during tree death after seawater exposure. Based on our study, likely mechanisms of carbon starvation in these trees include the dramatic declines in whole-tree photosynthesis due to reduced leaf-level gas exchange from constrained stomatal conductance associated with hydraulic limitations (Figure 5), along with cellular ion toxicity (Figure 6), and finally, large reductions in crown foliage (Figure 1).

High Na^+ stress-induced cellular promotes mortality

Osmotic adjustment maintains a minimal level of turgor required for tree survival and growth (Nguyen et al., 2017), and can function in coordination with declines in whole-plant hydraulic conductance under exposure to salinity (Mendez-Alonzo et al., 2016). Through the P–V relationships, we found that π_{tlp} increased during salinity–stress-induced tree death (Figure 3C). This is inconsistent with previous studies in seawater-adapted mangroves (Nguyen et al., 2017; Suárez and Sobrado, 2000), which found that π_{tlp} was lower (more negative) due to shifts in π_0 or ε with

Downloaded from https://academic.oup.com/plphys/article/187/2/873/6307737 by guest on 18 April 2024

increasing salinity (Nguyen et al., 2017). However, neither π_0 nor ε changed during the mortality process in our study (Supplemental Figure S1). Plants typically keep lower (more negative) π_{tlp} to maintain stomatal conductance, hydraulic conductance, and photosynthetic gas exchange when droughts occur, which is important for drought tolerance (Bartlett et al., 2012; Zhu et al., 2018). Apparently, the non-halophytic spruce trees in our study cannot acclimate to strong salinity stress (Byrt and Munns, 2008; Munns and Tester, 2008). Coastal trees not only need to handle the limited water absorption under high salinity but must also cope with the special challenges for the maintenance of favourable water and ion balances. In addition to higher π_{tlp}, RWC_{tlp} decreased with the decline of live foliated crown in our study (Figure 3; Supplemental Figure S1). This "wrong way" response is the opposite of osmotic acclimation and strongly suggests loss of osmotic responsiveness consistent with loss in integrity of the plasma membrane through toxic effects of salt accumulation within leaves. This is also a difference between mangroves adapted to salinity exposure in contrast to Sitka spruce which, though a coastal species, requires more fresh water in the soil to survive.

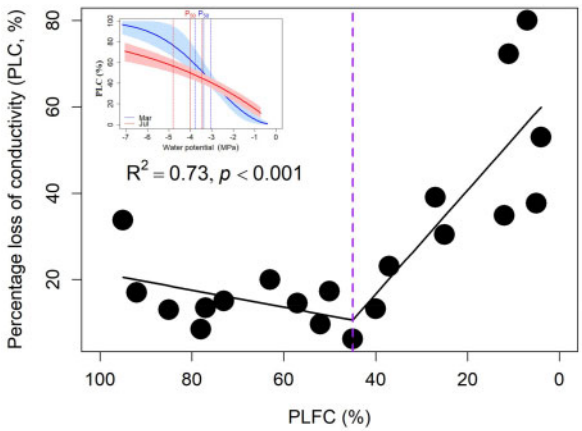

Figure 4 Relationship between native PLC and PLFC. A segmented model with break-point estimation is fitted to the data from the "Segmented" package in program R version 3.5.3. Change-point x = 45% was shown with a purple dashed line. Insert: Vulnerability curves of sitka-spruce (*Picea sitchensis*) generated in March and July. The water potential at 50% of conductivity lost (P_{50}) are −3.38 MPa and −4.00 MPa for March (is shown with solid blue line) and July (is shown with solid red line), respectively. The confidence intervals of the regressions are shown in light blue and light red color, respectively. The 95% confidence interval for P_{50} are shown with dashed lines. The curves were fitted using R package "fitplc."

We observed weak osmotic regulation ability in spruce trees and they were unable to maintain turgor and hydration under seawater exposure. This failure of osmotic adjustment was strongly related to Na^+ accumulation within trees, as reflected in significant correlations between foliar Na^+ concentration and key hydraulic traits (K_s, PLC, and π_{tlp}; Figure 6). Furthermore, no significant variation was observed in the predawn and midday leaf water potential during the study (across March to August) or in relation to crown decline despite the increase in soil porewater salinity from 7.16 to 13.90 PSU, which should cause a decrease in osmotic potential from −0.49 to −0.95 MPa (Figure 2; Supplemental Table S1). Additionally, vulnerability curves indicated that the values of P50 (−3.38 MPa and −4.00 MPa for March and July, respectively) were much lower than any of the predawn or midday leaf water potential values. Because the trees exhibited many physiological impacts before experiencing high PLC, this indicates that loss in cellular function reached a critical threshold before the precipitous loss in PLC. Therefore, it appears that these spruce trees have gone through the rapid osmotic phase of stress and are currently in the slower ionic phase (Munns and Tester, 2008). That is, trees lost the ability to exclude major ions over time, and high Na^+ stress-induced cellular injury in dying trees. To provide more evidence to determine the contribution of foliar Na^+ to the key plant functional traits during tree death, we conducted a PCA (Figure 7). The results showed that 88.2% of the total variance of the first PC axes were significantly correlated with foliar Na^+ concentration, which additionally confirmed our above analysis and provides a better view of the breaking points in which salinity promotes mortality.

Conclusions

The manipulation of the floodplain ecosystem from freshwater to tidally influenced salt deposition in 2014 promoted the death of coastal spruce trees, providing us with a unique

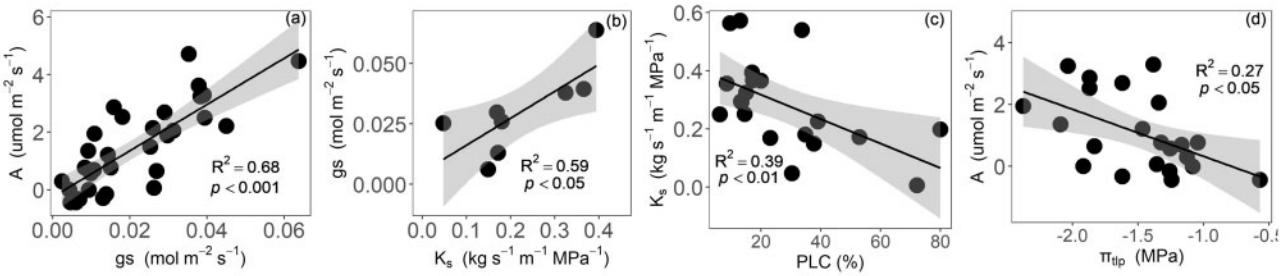

Figure 5 Relationships across key functional traits. Relationship between carbon assimilation rate (A) and stomatal conductance (gs; A); between gs and sapwood-specific hydraulic conductivity (K_s; B); between K_s and native PLC (C); and between A and turgor loss point (π_{tlp}; D). A linear model is fitted to the data. The points represent the individual trees. The confidence interval of the linear regression is shown in light grey color. The coefficients of determination and P-value are also shown.

Downloaded from https://academic.oup.com/plphys/article/187/2/873/6307737 by guest on 18 April 2024

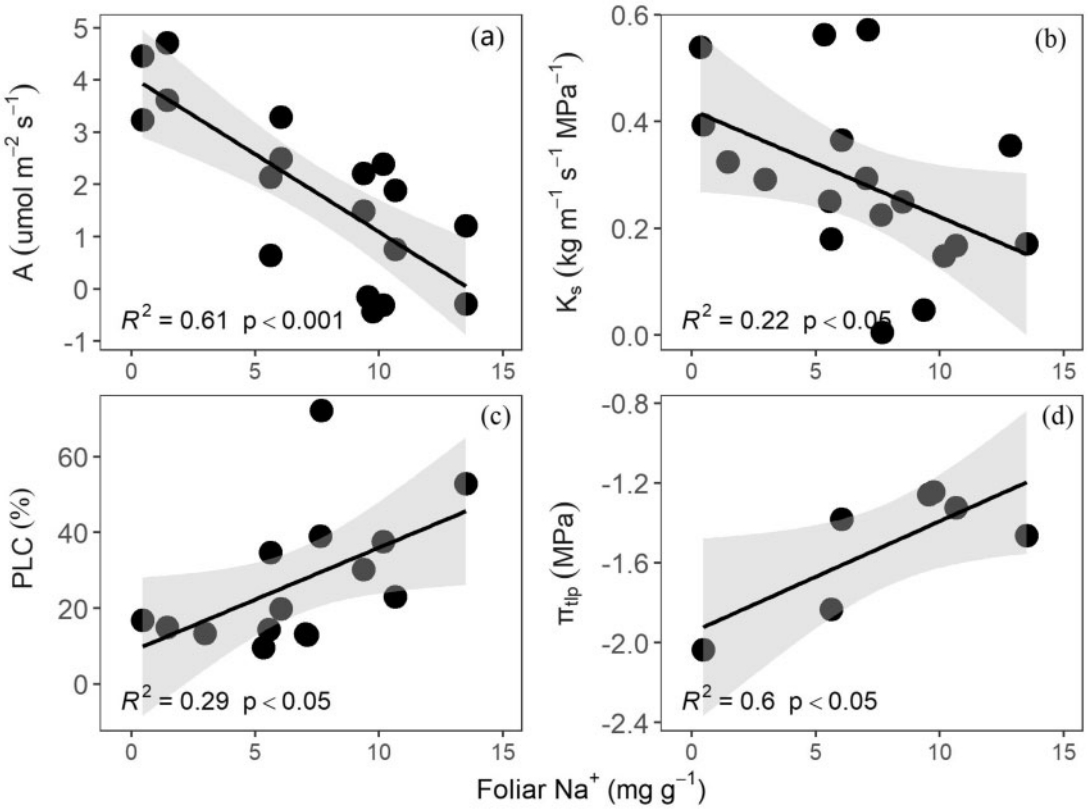

Figure 6 Relationship between foliar Na^+ concentration and tree key functional traits. Traits are carbon assimilation rate (*A*; A), sapwood-specific hydraulic conductivity (K_s; B), native PLC (C), and turgor loss point (π_{tlp}; D). A linear model is fitted to the data in each panel. The points represent the individual trees. The confidence intervals of the linear regressions are shown in light gray color. The coefficients of determination and *P*-values are also shown.

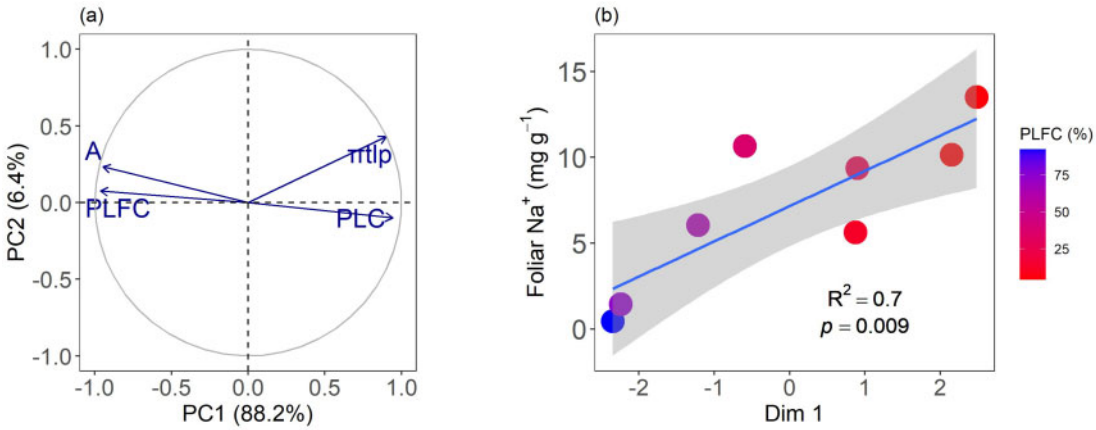

Figure 7 PCA for tree functional traits, foliar Na^+ concentration, and crown mortality. A, PCA based on three key functional traits and different crown status (live foliated crown condition, PLFC). The percentages in the axis labels indicate the variance explained by the axis. PC axes 1 and 2 explain 88.2% and 6.4% of the total variation, respectively. *A*: carbon assimilation rate; π_{tlp}: osmotic potential at turgor loss point. (B) Linear regression showed that the first component of PC axis (Dim 1) correlated with foliar Na^+ concentration ($P < 0.05$) among different levels of PLFC (from healthy trees to dying trees, as color from blue to red). The key functional trait data for analysing was measured in July, and the π_{tlp} were the mean values of measurements in June and August.

opportunity to observe the dynamic process of tree mortality in the field. Our results provide experimental evidence that seawater exposure induced losses of crown foliage, gas exchange, hydraulic, and osmotic traits before mortality in this ecosystem. The declining gas exchange was related to stem hydraulic loss and leaf osmotic damage under seawater exposure. Meanwhile, increased soil porewater salinity caused high Na^+ concentration stress and cellular injury,

Downloaded from https://academic.oup.com/plphys/article/187/2/873/6307737 by guest on 18 April 2024

induced osmotic dysfunction, and impaired hydraulic function, which most likely drove the rapid loss of crown foliage. Our observations provide strong evidence of toxic effects of ion accumulation on maintenance of cellular function, cellular injury, and death led to hydraulic system damage in dying trees. The ecosystem-manipulation upon which we derived our measurements provides a way to analyze death processes over short time scales, while over longer timescales, sea level rise has been demonstrated to similarly kill off upland forests and create "ghost forests" (e.g. Kirwan and Gedan 2019). Extensive sea-level rise in upcoming decades will create more ghost forests. Our findings provide a critical understanding of seawater exposure-induced mortality and highlight that cellular function injury under high salinity accumulation leads to incipient mortality, which promotes important insights for future mortality projections in coastal areas under climate change.

Materials and methods

Field site information

The study site was located along Beaver Creek (46° 54′ 25″ N, 123° 58′ 33″ W), a first-order tidal creek that drains into Johns River on the western coast of Washington State, USA (described in Zhang et al. 2021b). Beaver Creek is ∼1.5 km from Grays Harbor and 14.5 km from the Pacific Ocean. The field site is characterized by a mild, wet climate with a mean annual temperature and precipitation of 10.4°C and 1920 mm (during the period 1980–2017), respectively. Meterological data (air temperature rainfall and relative humidity (RH)) were monitored throughout the study period in the center of the study floodplain using a HOBO Micro Station Logger equipped with plug-and-play smart sensors for rain, temperature, and RH sensors (Onset Computer Corporation, Bourne, MA, USQ). Mean annual temperature in 2019 was 9.8°C at the study site, with mean monthly temperature ranging from 1.9°C in February to 17.0°C in August (Supplemental Figure S2). Annual precipitation in 2019 was 1,376 mm, with total monthly precipitation lowest in June (16 mm). Total daily radiation was lowest in December (0.25 MJ m^{-2}) and highest in June 2019 (30.06 MJ m^{-2}).

The coastal forest lies on a floodplain that did not experience flooding or seawater exposure until 2014 due to two culverts near the confluence of Beaver Creek that prevented seawater invasion but allowed freshwater drainage out of the creek (Washington Department of Fish and Wildlife (WDFW), 2019). In 2014, the culverts were removed for fish habitat restoration (Wang et al., 2019; Ward et al., 2019; Sengupta et al., 2019). Now, the trees experience seawater exposure from daily tidal exposure of ∼2 m in the adjacent stream, and approximately monthly extreme flooding events that saturate the floodplain for extended periods. High tides that inundate the site typically occurred with monthly regularity. The soil salinity also varied seasonally, with lower salinity occurring in winter and higher in summer. Maximum surface water salinity can reach 30 PSU at high tide in this area (Sengupta et al., 2019; Yabusaki et al., 2020). Since 2014, tree growth has slowed and mortality has increased in the floodplain Sitka-spruce trees (*Picea sitchensis*, the dominant tree species in the Pacific Northwest; Wang et al., 2019; Ward et al., 2019).

Determination of PLFC and tree sampling

At the beginning of the study (March 2019), we surveyed and recorded mortality and the crown mortality conditions (PLFC; %) of Sitka-spruce trees along an ∼ 800-m transect from along the Beaver Creek floodplain (Figure 1). The PLFCs were estimated based on needle browning and leaf shedding (crown "greenness," which is the percentage of the total branched canopy that holds live foliage; the same approach used in Gaylord et al., 2013 and Poyatos et al., 2013). Trees were considered alive when green needles were present. A tree was recorded as dead when there was no live foliated crown (the PLFC was 0%; Gaylord et al., 2013). The PLFC for each tree was the average of estimates from the same three to five researchers from three directions surrounding the tree on each date, to increase comparison accuracy across individual trees and months. During each campaign over the entirety of the study period (March to August 2019), we recorded PLFC and collected samples (healthy branches) from the trees along a gradient of PLFC from 7% to 95% for gas exchange, hydraulics, and other functional traits measurements (Supplemental Table S2). Noteably, the number of measured trees decreased during the year due to the rapid decline in the crown condition (some of the trees completely died during the study).

Floodplain soil porewater salinity measurements and modeling

We measured soil porewater in a shallow well located in the center of the floodplain (38 m inland from the creek) to provide empirical salinity trends during the study. The porewater salinity was monitored at 30-min frequency from April 2018 to August 2019. The well was 1-m deep, 2-in diameter PVC with 2.5 mm slots at 1-cm intervals across the entire belowground length (ESP Supply). The well was screened using 250-μm well socks (ESP Supply) and sealed at the ground surface with bentonite clay to reduce artifacts of infiltration during flood events. Electrical conductivity readings from deployed devices (HOBO U24-002 Conductivity, Onset Computer Corporation) were converted to salinity following standard UNESCO/IOC/SCOR/IAPSO procedures as defined in the International Thermodynamic Equation Of Seawater – 2010 (IOC et al. 2010) using the Gibbs SeaWater Oceanographic Toolbox written for R ("gsw" package; Kelley et al. 2017; Yabusaki et al., 2020). Salinity data were collected on 30-min intervals.

In addition to sensor measurements, we utilized a reactive transport model to estimate soil porewater salinity near each studied tree at depths of 0.05, 0.15, 0.25, 0.35, and 0.45 m. The restoration of tidal access to Beaver Creek in 2014 allowed seasonally varying salinity (1–33 PSU) from the Grays Harbor estuary to propagate up Beaver Creek during

Downloaded from https://academic.oup.com/plphys/article/187/2/873/6307737 by guest on 18 April 2024

a rising tide, and freshwater baseflow to flow downstream during falling tide. The highest monthly tides are sufficient to partially inundate the floodplain leading to progressive salinization of the previously freshwater system. A three-dimensional variably saturated flow and salinity transport model of the floodplain (Yabusaki et al., 2020) was developed using the PFLOTRAN Richards Equation simulator (Hammond et al., 2014) to simulate tree-specific soil porewater salinity from May 2015 to April 2019. The subsurface (<45 cm) salinity was modeled as our sampling trees were distributed on the same floodplain. Depth-resolved (0.05, 0.15, 0.25, 0.35, and 0.45-m depth) time histories of porewater salinity at each tree location were part of the model output generated at an hourly frequency with 3-m lateral and 0.1-m vertical resolution. We averaged the salinity from different depths as the tree-specific soil porewater salinity. The model results were validated against our continuous time-series data from our primary well (described above) as well as with measured water levels and salinity from the nearby creek and two additional floodplain wells (Yabusaki et al. 2020). A more detailed description of the modeling can be found in Yabusaki et al. (2020) at this site.

Leaf gas exchange

We measured leaf gas exchange parameters, including carbon assimilation rate (*A*), stomatal conductance (*gs*), and transpiration rate (*E*) by using a portable gas exchange system (LI-6800, LI-COR Inc., Lincoln, NE, USA) with a 6 cm^2 combined light source leaf chamber, monthly from May to August 2019 on sunny days from 09:00 to 14:00. A 20-m pole pruner was used to cut three >1-m long branches from each tree, cut ends were covered with wet towels and put in the plastic bags, and gas exchange measurements were measured immediately on the small twig (with approximately 30 needles) from each branch. Gas exchange measurements closely followed the approach recently described by Wu et al. 2019 and 2020. Specifically, the chamber conditions were kept close to ambient by matching air temperature and relative humidity. For each measurement, we set chamber CO_2 concentration to 400 ppm and the photosynthetically active radiation to 1,200 μmol m^{-2} s^{-1}. Measurements were conducted at a flow rate of 500 μmol s^{-1}. After clamping a small twig in the chamber, we checked the chamber for leaks and putty (Qubitac) was used to seal the chamber if the leak was >5%. We logged data three to five times after *A* and *gs* reached stability within 5 min to maximize representation of ambient conditions during measurement. The foliage enclosed within the 6,800 chambers was photographed and its leaf area was measured using Image-J software (US National Institutes of Health, Bethesda, MD, USA). The gas exchange data were corrected by leaf area.

Leaf water potential

We measured leaf water potential monthly in the field from March to August (except April) 2019 with a pressure chamber (Model 1505-D; PMS Instruments, Albany, OR, USA) to determine water status. Branch samples for predawn (Ψ_{pd}; MPa) and midday (Ψ_{md}; MPa) water potential were collected before sunrise (04:00–06:00) and at midday (12:00–14:00), respectively. Two or three branches from each were cut using a pole pruner. Water potential was measured by using two or three twigs excised from the larger branches, and the ends were cleanly cut with a fresh razor blade for better visualization (Hochberg, 2019).

Foliar sodium (Na^+) concentration

We measured foliar sodium (Na^+) concentration with ion coupled plasma optical emission spectrometry (ICP-OES, 7300 DV, Perkin Elmer, MA, USA) after acid digestion. Specifically, samples were weighed into tared clean polyethylene vials. We added 4-mL trace metal-free (TMF) concentrated nitric acid to samples and allowed to sit for 1 h. Samples were then heated for 6 h at 80°C. Samples sat overnight after heating. Then added 5-mL TMF concentrated hydrochloric acid to the samples, and samples were digested for 6 h at 85°C. After samples were cooled and 3 mL of TMF hydrogen peroxide was added, we heated samples at 80°C for 1.5 h. After these digestion steps, samples were cooled and 60 mL of DI water was added. The final sample was then weighed and subtracted from the tare weight to calculate the mass of the digestates and ultimately the density of the digestate. The samples were allowed to sit overnight to settle any remaining particles and decanted for analysis. Blank samples with 60 mL of DI water were also subjected to the same procedures as above using only the solvents and no solid matrix.

In samples with low Na^+ concentration, the samples were re-analyzed in an axial mode for better sensitivity. A two-point calibration was used, a blank and a high standard. The calibration was verified using a second source standard for all analyzed analytes. Continuing calibration verification standards and blanks were run every 10 samples, to ensure that the analytical system was operating properly. We added an internal standard online to correct for any matrix effect from the samples. Method blanks were below detection limits. Data are reported as mg g^{-1} dry weight in this study.

Stem hydraulic conductivity and vulnerability curves

We measured hydraulic conductivity and vulnerability curves in March and July 2019. We collected ~1.5-m-long healthy branches from the individual trees with different PLFC using a 5-m-high pole pruner in the field. Cut ends were covered with parafilm and samples were placed in large opaque plastic bags with wet towels to prevent the samples from drying out, then transported to the laboratory. Once in the laboratory, a stem segment (~14 cm in length and 5–8 mm in diameter) was excised under water immediately after a branch was taken out from the bag for native hydraulic conductivity (K_h; kg m s^{-1} MPa^{-1}) measurements. We trimmed off ~1-cm bark at each end of the segment under water. After making a final, clean cut on each end with a fresh razor blade, the segment was connected to a

Downloaded from https://academic.oup.com/plphys/article/187/2/873/6307737 by guest on 18 April 2024

tubing system and perfused with degassed and filtered mineralized water (20 mM KCl). A constant hydraulic head of 50 cm ($\triangle P$; MPa) was used to generate pressure that drove the solution flow through the segments and avoid flushing native embolism. The solution then flowed into a reservoir on an analytical balance (±0.1 mg; Secura 225D-1S; Sartorius), and the weight was recorded by a computer (Sperry et al., 1988a). We corrected for stem passive water uptake by beginning and ending each conductance measurement with a "background" measurement (Torres-Ruiz et al., 2012). K_h was calculated as:

$$K_h = F \times L/\Delta P \quad (1)$$

where F was the flow of water through the stem (F; kg s^{-1}), L is the stem length (m), and ΔP is the driving force (MPa). Hydraulic conductivity was also normalized by sapwood area (A_{sw}; m^2) to calculate sapwood-specific hydraulic conductivity (K_s; kg m^{-1} s^{-1} MPa^{-1}). Sapwood area was determined at both ends of the segment.

After measurement of native K_h, the segments were submerged in degassed solution (20 mM KCl) under vacuum infiltration overnight (>12 h) to remove emboli in tracheids. Before maximum hydraulic conductivity (K_{max}), the stem segments were trimmed to confirm the absence of bubbles at the cut ends under the degassed solution. K_{max} was measured as above for K_h measurement. The native percentage loss of conductivity (PLC) was calculated as:

$$\mathrm{PLC} = 100 - (1 - (K_h/K_{max}))$$

(2)Vulnerability to cavitation was determined by creating vulnerability curves using the bench dehydration method (Cochard et al., 2010; Sperry et al., 1988b). We collected four to six stem xylem segments from each long branches of individuals for K_h and K_{max} measurements. At the same time, we cut three small twigs from the branch and put them each in a plastic bag to equilibrate for 15 min, then measured their water potential with a pressure chamber. We let the branch samples dry on the bench. The measurements of K_h, K_{max}, and water potential were continued until the stem lost >90% conductivity or the water potential less than −8 MPa. A reparameterized Weibull model was used to generate vulnerability curves by fitting water potential versus PLC data points (Neufeld et al., 1992; Ogle et al., 2009) from the "FITPLC" package in program R version 3.5.3 (Duursma and Choat, 2017). The water potential at 50% of conductivity lost (P_{50}) was determined for each month from this model.

Leaf pressure–volume relationships

Leaf P–V curves were measured May, June, and August 2019 using the bench drying technique (Tyree and Hammel, 1972). Three twigs (~15 cm) of each were cut from >1 m branches that were used for predawn water potential measurements. The twigs were put in Whirl-Pak bags with the cut end in water during transport to the laboratory. Before the determination of P–V relationships, the twigs were recut under water and allowed to rehydrate overnight. Leaf fresh weight was measured with an analytical balance and water potential was measured with a pressure chamber periodically during slow desiccation of the samples on the bench. At the end of this process, the samples were dried in an oven at 70°C for 48 h for dry mass determination. P–V curves were constructed for each twig to estimate osmotic potential at full turgor (π_0; MPa), turgor loss point (π_{tlp}; MPa), SWC (g g^{-1}), relative water content at the turgor loss point (RWC_{tlp}; MPa), modulus of elasticity (ε; MPa). Plotting the inverse of water potential against RWC allowed the determination of the π_{tlp} as the point of transition between linear and nonlinear portions. We estimated π_0 by extrapolating the straight-line section to 100% RWC, and SWC was the ratio of water mass to leaf dry mass in a fully saturated leaf. We determined ε from the slope of the pressure potential between π_0 and π_{tlp}, and ε estimates cell wall rigidity averaged across the leaf. The "*water_mass. R*" and "*pvc_fitting_v4. R*" functions were used to generate P–V curves in R version 3.5.3.

Statistical analysis

We used repeated-measures ANOVA to test differences of PLFC and soil porewater salinity among months. We used linear mixed-effect (LME) models to evaluate the relationships (1) between soil porewater salinity, gas exchange parameters (A), water potential (Ψ_{pd} and Ψ_{md}), K_s, P–V parameters (π_0, π_{tlp}, SWC, RWC_{tlp}, and ε), and PLFC; (2) between A and gs, gs and K_s, K_s and PLC, A and π_{tlp}; (3) between A, K_s, PLC, π_{tlp}, and foliar Na^+ concentration. In our models, we considered the different individuals as a random factor. The differences of A, K_s, π_{tlp} among/between months were tested by ANOVA or student's t test. A regression model with change-point estimation with R package "segmented" (version 1.1-0) was used to fit the relationship between PLC and PLFC. In addition, we conducted PCA based on four key functional traits and eight individuals measured all these four functional traits to investigate multivariate associations among all variables. We also extract the first component of the axis (Dim 1), and correlated it with foliar Na^+ concentration using LME models. All statistical analysis was performed using R statistical software (version 3.5.3; R Core Team, 2018). Results were considered statistically significant at $P < 0.05$.

Supplemental data

The following materials are available in the online version of this article.

Supplemental Figure S1. Relationship between osmotic potential at full turgor (π_0), SWC, RWCtlp, and modulus of elasticity (ε) and PLFC.

Supplemental Figure S2. Meteorological data in the site.

Supplemental Table S1. Mean porewater salinity and the equivalent seawater osmotic potential for PSU of River Bank by month (March–August) in the year 2019.

Downloaded from https://academic.oup.com/plphys/article/187/2/873/6307737 by guest on 18 April 2024

Supplemental Table S2. Sample size and monthly measured information for all parameters.

Acknowledgments

We thank Heather Pacheco, James Abend, and Dakotah DeRoos for their assistance in field sampling and in laboratory; Don Lentz, the Hancock Timber Company, and Washington Department of Fish and Wildlife for access to the Beaver Creek field site; and the support from the Ecoclimatology research group and Shapotou Desert Research and Experiment Station. This research is part of the PREMIS Initiative at Pacific Northwest National Laboratory (PNNL). The project was conducted under the Laboratory Directed Research and Development Program at PNNL, a multiprogram national laboratory operated by Battelle for the U.S. Department of Energy.

Funding

This work was supported by the National Natural Science Foundation of China (grant nos. 4162001 and 41975150; to H.Z.), by the Chinese Academy of Sciences scholarship for overseas research (to H.Z.), and the Laboratory Directed Research and Development Program at Pacific Northwest National Laboratory PNNL under contract DE-AC05-76RL01830.

Conflict of interest statement. None declared.

References

Abou Jaoude R, de Dato G, Palmegiani M, De Angelis P (2013) Impact of fresh and saline water flooding on leaf gas exchange in two Italian provenances of *Tamarix africana* Poiret. Plant Biol **15**: 109–117

Adams HD, Zeppel MJB, Anderegg WRL, Hartmann H, Landhausser SM, Tissue DT, Huxman TE, Hudson PJ, Franz TE, Allen CD, et al. (2017) A multi-species synthesis of physiological mechanisms in drought-induced tree mortality. Nat Ecol Evol **1**: 1285–1291

Arsova B, Foster KJ, Shelden MC, Bramley H, Watt M (2020) Dynamics in plant roots and shoots minimize stress, save energy and maintain water and nutrient uptake. New Phytol **225**: 1111–1119

Ball MC, Farquhar GD (1984) Photosynthetic and stomatal responses of the grey mangrove, avicennia marina, to transient salinity conditions. Plant Physiol **74**: 7–11

Bartlett MK, Scoffoni C, Sack L (2012) The determinants of leaf turgor loss point and prediction of drought tolerance of species and biomes: a global meta-analysis. Ecol Lett **15**: 393–405

Bose J, Munns R, Shabala S, Gilliham M, Pogson B, Tyerman SD (2017) Chloroplast function and ion regulation in plants growing on saline soils: lessons from halophytes. J Exp Bot **68**: 3129–3143

Boursiac Y, Chen S, Luu D-T, Sorieul M, van den Dries N, Maurel C (2005) Early effects of salinity on water transport in arabidopsis roots. Molecular and cellular features of aquaporin expression. Plant Physiol **139**: 790–805

Brodribb TJ, Cochard H (2009) Hydraulic failure defines the recovery and point of death in water-stressed conifers. Plant Physiol **149**: 575–584

Brodribb TJ, Holbrook NM (2003) Stomatal closure during leaf dehydration, correlation with other leaf physiological traits. Plant Physiol **132**: 2166–2173

Brugnoli E, Lauteri M (1991) Effects of salinity on stomatal conductance, photosynthetic capacity, and carbon isotope discrimination of salt-tolerant (*Gossypium hirsutum* L.) and salt-sensitive (*Phaseolus vulgaris* L.) C(3) non-halophytes. Plant Physiol **95**: 628–635

Burchett MD, Field CD, Pulkownik A (1984) Salinity, growth and root respiration in the grey mangrove, Avicennia marina. Physiol Plantarum **60**: 113–118

Byrt CS, Munns R (2008) Living with salinity. New Phytol **179**: 903–905

Cochard H, Herbette S, Barigah T, Badel E, Ennajeh M, Vilagrosa A (2010) Does sample length influence the shape of xylem embolism vulnerability curves? A test with the Cavitron spinning technique. Plant Cell Physiol **33**: 1543–1552.

Delfine S, Alvino A, Villani MC, Loreto F (1999) Restrictions to carbon dioxide conductance and photosynthesis in spinach leaves recovering from salt stress. Plant Physiol **119**: 1101–1106

Desantis LRG, Bhotika S, Williams K, Putz FE (2007) Sea-level rise and drought interactions accelerate forest decline on the Gulf Coast of Florida, USA. Glob Change Biol **13**: 2349–2360

Doyle TW, Krauss KW, Conner WH, From AS (2010) Predicting the retreat and migration of tidal forests along the northern Gulf of Mexico under sea-level rise. Forest Ecol Manag **259**: 770–777

Duursma R, Choat B (2017) fitplc - an R package to fit hydraulic vulnerability curves. J Plant Hydraulics **4**: 002.

Epstein E, Norlyn JD, Rush DW, Kingsbury RW, Kelley DB, Cunningham GA, Wrona AF (1980) Saline culture of crops: a genetic approach. Science **210**: 399–404

Ewers FW, Lopez-Portillo J, Angeles G, Fisher JB (2004). Hydraulic conductivity and embolism in the mangrove tree *Laguncularia racemosa*. Tree Physiol **24**: 1057–1062

Foster GL, Rohling EJ (2013) Relationship between sea level and climate forcing by CO2 on geological timescales. Proc Natl Acad Sci U S A **110**: 1209–1214

Gaylord ML, Kolb TE, Pockman WT, Plaut JA, Yepez EA, Macalady AK, Pangle RE, McDowell NG (2013) Drought predisposes piñon–juniper woodlands to insect attacks and mortality. New Phytol **198**: 567–578

Gong L, Liu XD, Zeng YY, Tian XQ, Li YL, Turner NC, Fang XW (2021) Stomatal morphology and physiology explain varied sensitivity to abscisic acid across vascular plant lineages. Plant Physiol **186**: 782–797

Hammond GE, Lichtner P C, Mills RT (2014) Evaluating the performance of parallel subsurface simulators: an illustrative example with PFLOTRAN. Water Resour Res **50**: 208–228

Hao GY, Jones TJ, Luton C, Zhang YJ, Manzane E, Scholz FG, Bucci SJ, Cao KF, Goldstein G (2009) Hydraulic redistribution in dwarf Rhizophora mangle trees driven by interstitial soil water salinity gradients: impacts on hydraulic architecture and gas exchange. Tree Physiol **29**: 697–705

Harvey HW (1966) The Chemistry and Fertility of Sea Waters. Cambridge University Press, Cambridge, MA

Hauser F, Horie T (2010) A conserved primary salt tolerance mechanism mediated by HKT transporters: a mechanism for sodium exclusion and maintenance of high K(+)/Na(+) ratio in leaves during salinity stress. Plant Cell Physiol **33**: 552–565

Hochberg U (2019) Letter to the editor facilitating protocols while maintaining accuracy in grapevine pressure chamber measurements-comments on Levin 2019. Agr Water Managt **227**: 105836

Horie T, Hauser F, Schroeder JI (2009) HKT transporter-mediated salinity resistance mechanisms in Arabidopsis and monocot crop plants. Trends Plant Sci **14**: 660–668

James RA, Rivelli AR, Munns R, Caemmerer Sv (2002) Factors affecting CO2 assimilation, leaf injury and growth in salt-stressed durum wheat. Funcl Plant Biol **29**: 1393

Jevrejeva S, Jackson LP, Riva EM, Grinsted A, Moore JC (2016) Coastal sea level rise with warming above 2 degrees C. Proc Natl Acad Sci U S A **113**: 13342–13347

Downloaded from https://academic.oup.com/plphys/article/187/2/873/6307737 by guest on 18 April 2024

Kaneko T, Horie T, Nakahara Y, Tsuji N, Shibasaka M, Katsuhara M (2015) Dynamic regulation of the root hydraulic conductivity of barley plants in response to salinity/osmotic stress. Plant Cell Physiol **56**: 875–882

Kelley D, Richards C, SCOR/IAPSO W (2017) gsw: gibbs sea water functions. R package version 1.0-5. https://doi.org/https://CRAN.R-project.org/package=gsw (accessed October 2019)

Kirwan M, Gedan K (2019) Sea-level driven land conversion and the formation of ghost forests. Nat Clim Change **9**: 450–457

Langston AK, Kaplan DA, Putz FE (2017) A casualty of climate change? Loss of freshwater forest islands on Florida's Gulf Coast. Glob Change Biol **23**: 5383–5397

Laura LH, Anten NPR, Miguel MR, Ackerly DD (2007) Salinity and light interactively affect neotropical mangrove seedlings at the leaf and whole plant levels. Oecologia **150**: 545–556

Leopold A, Marchand C, Renchon A, Deborde J, Quiniou T, Allenbach M (2016) Net ecosystem CO2 exchange in the "Coeur de Voh" mangrove, New Caledonia: effects of water stress on mangrove productivity in a semi-arid climate. Agr Forest Meteorol **223**: 217–232

Li WB, Zhang HX, Wang WZ, Zhang PP, Ward ND, Norwood M, Meyers-Pigg A, Zhao CY, Leff RT, Yabusaki S, et al. (2021) Changes in carbon and nitrogen metabolism during seawater-induced mortality of Picea sitchensis trees. Tree Physiol https://doi.org/10.1093/treephys/tpab073

Liu X., Conner WH, Song B, Jayakaran AD (2017) Forest composition and growth in a freshwater forested wetland community across a salinity gradient in South Carolina, USA. Forest Ecol Manage **389**: 211–219

McDowell N, Beerling D, Breshears D, Fisher R, Raffa K, Stitt M (2011) Interdependence of mechanisms underlying climate-driven vegetation mortality. Trends Ecol Evol **26**: 523–532

Meehl GA, Washington WM, Collins WD, Arblaster JM, Hu A, Buja LE, Strand WG, Teng H (2005) How much more global warming and sea level rise? Science **307**: 1769–1772

Melcher PJ, Goldstein G, Meinzer FC, Yount DE, Jones TJ, Holbrook NM, Huang CX (2001) Water relations of coastal and estuarine Rhizophora mangle: xylem pressure potential and dynamics of embolism formation and repair. Oecologia **126**: 182–192

Mendez-Alonzo R, Lopez-Portillo J, Moctezuma C, Bartlett MK, Sack L (2016) Osmotic and hydraulic adjustment of mangrove saplings to extreme salinity. Tree Physiol **36**: 1562–1572

Miller G, Suzuki N, Ciftci-Yilmaz S, Mittler R (2010) Reactive oxygen species homeostasis and signalling during drought and salinity stresses. Plant Cell Physiol **33**: 453–467

Moradi F, Ismail AM (2007) Responses of photosynthesis, chlorophyll fluorescence and ROS-Scavenging systems to salt stress during seedling and reproductive stages in rice. Ann Bot **99**: 1161–1173

Munns R (2002) Comparative physiology of salt and water stress. Plant Cell Environ **25**: 239–250

Munns R (1993) Physiological processes limiting plant-growth in saline soils—some dogmas and hypotheses. Plant Cell Environ **16**: 15–24

Munns R, Day DA, Fricke W, Watt M, Arsova B, Barkla BJ, Bose J, Byrt CS, Chen ZH, Foster KJ, et al. (2020a) Energy costs of salt tolerance in crop plants. New Phytol **225**: 1072–1090

Munns R, Gilliham M (2015) Salinity tolerance of crops—what is the cost? New Phytol **208**: 668–673

Munns R, Passioura JB, Colmer TD, Byrt CS (2020b) Osmotic adjustment and energy limitations to plant growth in saline soil. New Phytol **225**: 1091–1096

Munns R, Tester M (2008) Mechanisms of salinity tolerance. Annu Rev Plant Biol **59**: 651–681

Naidoo G (1987) Effects of salinity and nitrogen on growth and water relations in the mangrove, Avicennia-Marina (Forsk) Vierh. New Phytol **107**: 317–325

Neufeld HS, Grantz DA, Meinzer FC, Goldstein G, Crisosto GM, Crisosto C (1992) Genotypic variability in vulnerability of leaf xylem to cavitation in water-stressed and well-irrigated sugarcane. Plant Physiol **100**: 1020–1028

Nguyen HT, Meir P, Sack L, Evans J, Oliveira RS, Ball MC (2017) Leaf water storage increases with salinity and aridity in the mangrove *Avicennia marina*: integration of leaf structure, osmotic adjustment and access to multiple water sources. Plant Cell Environ **40**: 1576–1591

Ogle K, Barber JJ, Willson C, Thompson B (2009) Hierarchical statistical modeling of xylem vulnerability to cavitation. New Phytol **182**: 541–554

Parida AK, Das AB (2005) Salt tolerance and salinity effects on plants: a review. Ecotox Environ Safe **60**: 324–349

Pedrero F, Maestre-Valero JF, Mounzer O, Alarcon JJ, Nicolas E (2014) Physiological and agronomic mandarin trees performance under saline reclaimed water combined with regulated deficit irrigation. Agr Water Manage **146**: 228–237

Poyatos R, Aguadé D, Galiano L, Mencuccini M, Martínez-Vilalta J (2013) Drought-induced defoliation and long periods of near-zero gas exchange play a key role in accentuating metabolic decline of Scots pine. New Phytol **200**: 388–401

R Core Team (2018) *R: a Language and Environment for Statistical Computing*. R Foundation for Statistical Computing, Vienna, Austria

Sack L, Holbrook NM. 2006. Leaf hydraulics. Annu Rev Plant Biol **57**: 361–381

Schieder N, Kirwan M. 2019. Sea-level driven acceleration in coastal forest retreat. Geology **47**: 1151–1155

Scholander P (2006) How mangroves desalinate seawater. Physiol Plantarum **21**: 251–261

Sengupta A, Indivero J, Gunn C, Tfaily MM, Chu RK, Toyoda J, Bailey VL, Ward ND, Stegen JC (2019) Spatial gradients in the characteristics of soil-carbon fractions are associated with abiotic features but not microbial communities. Biogeosciences **16**: 3911–3928

Silliman BR, van de Koppel J, Bertness MD, Stanton LE, Mendelssohn IA (2005) Drought, snails, and large-scale die-off of southern U.S. salt marshes. Science **310**: 1803–1806

Sobrado MA (2001) Hydraulic properties of a mangrove *Avicennia germinans* as affected by NaCl. Biol Plantarum **44**: 435–438

Sperry JS, Donnelly JR, Tyree MT (1988a) A method for measuring hydraulic conductivity and embolism in xylem. Plant Cell Environ **11**: 35–40

Sperry JS, Tyree MT, Donnelly JR (1988b) Vulnerability of xylem to embolism in a mangrove vs an inland species of Rhizophoraceae. Physiol Plantarum **74**: 276–283

Suárez N, Medina E (2006) Influence of salinity on Na^+ and K^+ accumulation, and gas exchange in *Avicennia germinans*. Photosynthetica **44**: 268–274

Suárez N, Sobrado MA (2000) Adjustments in leaf water relations of mangrove (*Avicennia germinans*) seedlings grown in a salinity gradient. Tree Physiol **20**: 277–282

Thorne K, MacDonald G, Guntenspergen, et al. (2018) U.S. Pacific coastal wetland resilience and vulnerability to sea-level rise. Sci Adv **4**: 3270

Torres-Ruiz JM, Sperry JS, Fernández JE (2012) Improving xylem hydraulic conductivity measurements by correcting the error caused by passive water uptake. Physiol Plantarum **146**: 129–135

Twilley RR, Barron EJ, Gholz HL, Harwell MA, Zimmerman RJ (2001) Confronting climate change in the gulf coast region: prospects for sustaining our ecological heritage. Union of Concerned Scientists and The Ecological Society ofAmerica UCS Publication, Cambridge, MA

Tyree MT, Hammel HT (1972) The Measurement of the turgor pressure and the water relations of plants by the pressure-bomb technique. J Exp Bot **23**: 267–282

Vermeer M, Rahmstorf S (2009) Global sea level linked to global temperature. Proc Natl Acad Sci U S A **106**: 21527–21532

Downloaded from https://academic.oup.com/plphys/article/187/2/873/6307737 by guest on 18 April 2024

Wang W, McDowell NG, Ward ND, Indivero J, Gunn C, Bailey VL (2019) Constrained tree growth and gas exchange of seawater-exposed forests in the Pacific Northwest, USA. J Ecol **107**: 2541–2552

Ward ND, Indivero J, Gunn C, Wang WZ, Bailey V, McDowell NG (2019) Longitudinal gradients in tree stem greenhouse gas concentrations across six pacific northwest coastal forests. J Geophyl Res-Biogeo **124**: 1401–1412

Welfare K, Yeo AR, Flowers TJ (2002) Effects of salinity and ozone, individually and in combination, on the growth and ion contents of two chickpea (Cicer arietinum L.) varieties. Environ Pollut **120**: 397–403

Williams K, Ewel KC, Stumpf RP, Putz FE, Workman TW (1999) Sea-level rise and coastal forest retreat on the west coast of Florida, USA. Ecology **80**: 2045–2063

Wu J, Rogers A, Albert LP, Ely K, Prohaska N, Wolfe BT, Oliveira RC Jr, Saleska SR, Serbin SP (2019) Leaf reflectance spectroscopy captures variation in carboxylation capacity across species, canopy environment and leaf age in lowland moist tropical forests. New Phytol **224**: 663–674

Wu J, Serbin SP, Ely KS, Wolfe BT, Dickman LT, Grossiord C, Michaletz ST, Collins AD, Detto M, McDowell NG, et al. (2020) The response of stomatal conductance to seasonal drought in tropical forests. Glob Change Biol **26**: 823–839

Yabusaki SB, Myers-Pigg AN, Ward ND, Waichler SR, Sengupta A, Hou Z, Chen X, Fang Y, Duan Z, Serkowski JA, et al. (2020) Floodplain inundation and salinization from a recently restored first-order tidal stream. Water Resour Res **56**: e2019WR026850

Yang YJ, Bi MH, Nie ZF, Jiang H, Liu XD, Fang XW, Brodribb TJ (2021) Evolution of stomatal closure to optimize water use efficiency in response to dehydration in ferns and seed plants. New Phytol **230**: 2001–2010

Yao GQ, Nie ZF, Turner NC, Li FM, Gao TP, Fang XW, Scoffoni C (2021) Combined high leaf hydraulic safety and efficiency provides drought tolerance in Caragana species adapted to low mean annual precipitation. New Phytol **229**: 230–244

Yeo AR, Leeks Izard, P, Bourssier PJ, Flowers TJ (1991) Short- and long-term effects of salinity on leaf growth in rice (*Oryza sativa L.*). J Exp Bot **42**: 881–889

Zhang HX, Yuan FH, Wu JB, Jin CJ, Pivovaroff AL, Yian JY, Li WB, Guan DX, Wang AZ, McDowell NG (2021a) Responses of functional traits to seven-year nitrogen addition in two tree species: coordination of hydraulics, gas exchange and carbon reserves. Tree Physiol **41**:190–205

Zhang PP, McDowell NG, Zhou XH, Wang WZ, Leff RT, Pivovaroff AL, Zhang HX, Chow PS (2021b) Declining carbohydrate content of Sitka-spruce trees dying from seawater exposure. Plant Physiol **185**: 1682–1696

Zhu SD, Chen YJ, Ye Q, He PC, Liu H, Li RH, Fu PL Jiang GF, Cao KF (2018) Leaf turgor loss point is correlated with drought tolerance and leaf carbon economics traits. Tree Physiol **38**: 658–663

Downloaded from https://academic.oup.com/plphys/article/187/2/873/6307737 by guest on 18 April 2024